03,08

# Thermoelectric properties of p-$(Bi,Sb)_2Te_3$ solid solution taking into account of the energy dependence of the relaxation time

© L.N. Lukyanova, O.A. Usov, V.A. Danilov

Ioffe Institute,
St. Petersburg, Russia

E-mail: lidia.lukyanova@mail.ioffe.ru

*Received October 23, 2024*
*Revised November 3, 2024*
*Accepted November 3, 2024*

The temperature dependences of thermoelectric properties in polycrystalline layered films of p-$Bi_{0.5}Sb_{1.5}Te_3$ topological insulators formed on polyimide and mica substrates by discrete deposition and thermal evaporation techniques have been studied. It is shown that the increase in the figure of merit Z of p-$Bi_{0.5}Sb_{1.5}Te_3$ depends on the value of the effective scattering parameter $r_{\text{eff}}$, which determines the energy dependence of the relaxation time $\tau(E)$. An increase in the figure of merit, up to $Z_{max} = 4.5 \cdot 10^{-3}\,\text{K}^{-1}$ at $T = 240\,\text{K}$, is observed at optimal values of the $r_{\text{eff}}$ parameter in the annealed films formed by discrete deposition on polyimide and mica substrates. Such enhancement of $Z$ in the film on the polyimide substrate is determined by a low thermal conductivity, and on the mica one by an increase in the power factor caused by raise of the Seebeck coefficient. Deviation from the optimal values of $r_{\text{eff}}$ in the unannealed films on polyimide during discrete evaporation results in a decrease in the figure of merit.

**Keywords:** chalcogenides of bismuth and antimony, the figure of merit, topological insulator, scattering parameter.

DOI: 10.61011/PSS.2024.12.60209.289

## 1. Introduction

Bismuth/antimony chalcogenide-based films are known not only as effective thermoelectric materials, but also as advanced three-dimensional (3D) topological insulators (TI) [1,2]. Topological surface states in TI are induced by inversion of the band gap edges as a result of strong spin-orbit interaction [3,4]. Bulk part becomes an insulator, and anomalous metallic conductivity of electrons with rigid coupling between the spin and pulse, that is typical of the Dirac fermions, occurs on the surface [1,2].

Properties of the Dirac fermions that are protected by time reversal symmetry against back scattering on non-magnetic defects define strong relaxation time dependence on energy [5–7]. Dirac fermion scattering mechanism and dependence $\tau(E)$ in TI were studied in [6,7] in terms of the non-equilibrium Boltzmann theory. For 3D-TI bismuth/antimony chalcogenides, time relaxation dependence on energy corresponds to short-range delta scattering and in the limiting case to $\tau(E) \propto E^{-1}$.

Strengthening of $\tau(E)$ comes with an increase in the Seebeck coefficient $S$ [5–7]. Moreover, growth of $S$ is defined by the energy filtration effect of charge carriers [4,8]. The energy filtration effect is associated with occurrence of potential barrier grains on interfaces with high-energy charge carriers passing through the barrier, thus, providing the growth of $S$, while low-energy carriers are filtered out [9].

Channels that provide higher mobility due to the absence of back scattering on non-magnetic defects may be formed in TI [10]. However, residual bulk conductivity due to the presence of bulk defects in TI [11,12] reduces the contribution of surface states to the total conductivity. Partial compensation of the bulk conductivity is achieved as a result of optimization of thermoelectric properties by changing TI composition and process variables [11].

The highest heat transfer in the films of interest is performed by long-wavelength phonons that mainly define the lattice thermal conductivity. At temperatures below room temperature, the lattice thermal conductivity $\kappa_{\text{L}}$ decreases due to phonon scattering on intercrystalline interfaces. In addition, decrease in $\kappa_{\text{L}}$ is associated with scattering on intrinsic acceptor antisite defects of bismuth in tellurium sites $Bi_{Te}$ and on impurity defects in atom substitutions $Sb \rightarrow Bi$ [13,14], and the contribution of phonon–phonon scattering grows in the vicinity of room temperature [15,16]. Lattice thermal conductivity is reduced additionally due to phonon scattering on Te(1) layer boundaries of the Van der Waals gaps that form a superlattice [17].

The TI properties mentioned above that define the increase in the Seebeck coefficient and the decrease in the thermal conductivity provide the growth of thermoelectric figure of merit in chalcogenide films despite the electric conductivity reduction.

This study investigates thermoelectric properties of submicron p-$Bi_{0.5}Sb_{1.5}Te_3$ TI films formed by the discrete and thermal evaporation methods using various substrates and heat treatment. Analysis of properties responsible for the thermoelectric figure of merit included the effective

scattering parameter $r_{\text{eff}}$ that defines the relaxation time dependence on energy.

## 2. Film fabrication technique and film structure

Polycrystalline films of the $(Bi,Sb)_2Te_3$ solid solutions were formed on mica and polyimide substrates by the discrete and thermal evaporation methods in an isothermal chamber that provided the vacuum of $1 \cdot 10^{-6}$ mmHg and thermal uniformity in the substrate plane. Film deposition by thermal evaporation involved placement of charge materials into a quartz crucible heated by the molybdenum coil radiation. Film deposition rate was 10–15 Å/s. For discrete evaporation, small batches of the feedstock powder with 10 $\mu$m grains were fed into the heated quartz crucible and evaporated immediately. Evaporator temperatures in the range of 800–850°C and a substrate temperature of 250–300°C are the best conditions for deposition of the $(Bi,Sb)_2Te_3$ films.

Thermoelectric materials based on $Bi_2Te_3$ have rhombohedral crystal structure that consists of flat anisotropic layers forming quintets separated by the Van der Waals gaps [18]. Quintets ($-Te^{(1)}-Bi-Te^{(2)}-Bi-Te^{(1)}$) are interconnected through weak Van der Waals forces which causes slight separation of thermoelectric materials in the (0001) planes that are perpendicular to the third-order crystallographic axis $c$. In the p-$Bi_{0.5}Sb_{1.5}Te_3$ solid solutions, Sb atoms substitute Bi atoms in the quintets. In the deposited polycrystalline p-$Bi_{0.5}Sb_{1.5}Te_3$ films, the (0001) plane has the lowest free energy, therefore Bi and Sb chalcogenide nuclei are formed with the prevailing orientation along the $c$ axis perpendicularly to the substrate plane [19,20].

Thermoelectric properties of films were studied in an isothermal cryostat chamber at $P = 10^{-6}$ mmHg. Electric conductivity was measured in the Van der Pauw configuration at direct current oriented along the (0001) film surface. For measuring the Seebeck coefficient by the differential method, the operating temperature gradient was equal to about 4°C/cm. When measuring the thermal conductivity coefficient using the procedure described in [21], substrate thermal conductivity is measured initially, for which an auxiliary layer with high thermal resistance and $S$-shape to reduce heat flux shunting is deposited on the substrate. Then after film deposition on the substrate, the same auxiliary layer was deposited in the film. Thermal conductivity coefficient of the film was calculated by the difference between the thermal conductivities of the film-substrate and substrate system.

## 3. Energy dependence of time relaxation

Analysis of thermoelectric properties of the p-$Bi_{0.5}Sb_{1.5}Te_3$ films included the effective carrier scattering parameter that defines the dependence of time relaxation on energy as $\tau = \tau_0 E^r$, where the constant $\tau_0$ is independent of the energy $E$, and $r$ is the current value of the effective scattering parameter $r_{\text{eff}}$ [22]. $r_{\text{eff}}$ together with the reduced Fermi level $\eta$ were determined by the least-square method from the experimental Seebeck coefficient $S(r, \eta)$ and degeneracy parameter $\beta(r, \eta)$. $\beta(r, \eta) = I_1^2/(I_0 \cdot I_2)$ was calculated within the multivalley energy spectrum model for isotropic carrier scattering from the expressions of isotropic conductivity multipliers $I_0$, Hall conductivity $I_1$ and magnetoconductivity $I_2$ [22].

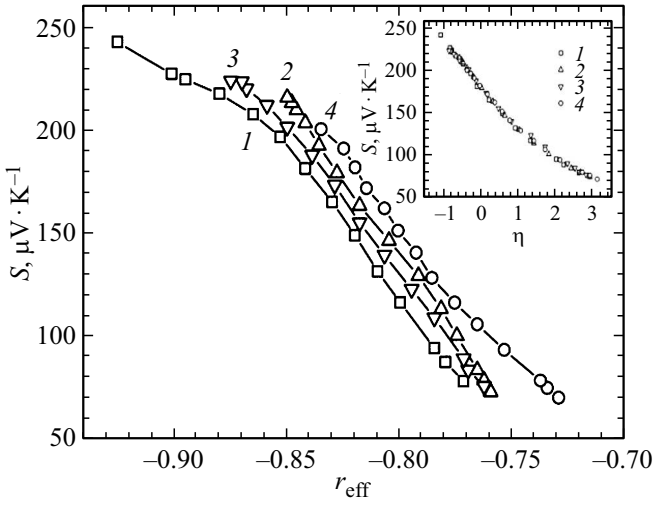


**Figure 1.** Dependences of the Seebeck coefficient $S$ on the effective carrier scattering parameter ($r_{\text{eff}}$) and reduced Fermi level $\eta$ (inset) in the p-$Bi_{0.5}Sb_{1.5}Te_3$ films. Curve *1* — discrete evaporation, unannealed polyimide substrate; *2* — discrete evaporation, annealed polyimide; *3* — discrete evaporation, annealed mica substrate; *4* — thermal evaporation, unannealed polyimide.

Submicron films investigated in this study have the bulk quadratic spectrum contribution to the energy dependence of time relaxation $\tau(E)$ [22] and linear component contribution due to surface states [6,7], therefore carrier scattering is described by $r_{\text{eff}}$ that takes into account the effective dependence $\tau(E)$, including both quadratic and linear spectra.

As shown in Figure 1, $|r_{\text{eff}}|$ increases as the Seebeck coefficient grows, which indicates that $\tau(E) \propto E^{r\text{eff}}$ is strengthened in the p-$Bi_{0.5}Sb_{1.5}Te_3$ films deposited at various process variables.

A value of $r_{\text{eff}}$ that is most close to the $(\tau(E) \propto E^{-1})$ limit (Figure 1, curve *1*) was measured in the unannealed p-$Bi_{0.5}Sb_{1.5}Te_3$ film with discrete evaporation to the polyimide substrate at $r_{\text{eff}} = (-0.925)-(-0.77)$. In such films, the Dirac point is placed near the valence band edge according to the scanning tunnel spectroscopy data [23] and $\tau(E)$ becomes close to the limit. Difference of $r_{\text{eff}}$ from $-1$ in films in Figure 1 might be associated with fluctuations induced by the effect of bulk carriers [5,24]. A dependence was detected according to which reduction

of $|r_{\text{eff}}|$ comes with the reduction of the Seebeck coefficient in the p-$Bi_{0.5}Sb_{1.5}Te_3$ films formed using various deposition and heat treatment methods (Figure 1).

## 4. Seebeck coefficients, electric conductivity and power factor

thermoelectric properties in the dependences on temperature were studied on the $t = (1.5-2)\,\mu$m p-$Bi_{0.5}Sb_{1.5}Te_3$ films. Surface states of the Dirac fermions might be observed in samples with a thickness of hundreds of nanometers [25] and even in samples with a thickness of several microns [5,26] due to high quantum phase coherence $l_\phi$ compared with the free fermion range $l_F$. In the studied p-$Bi_{0.5}Sb_{1.5}Te_3$ TI films, existence of surface states of the Dirac fermions is supported by the studies of differential tunnel conductivity by the scanning tunnel spectroscopy method [23] according to which the surface concentration of fermions reaches $n_s = 4 \cdot 10^{12}\,\text{cm}^{-2}$.

Figure 2, curves *1–4* and *6–8*, shows the temperature dependences of the Seebeck coefficient $S$ and electric conductivity $\sigma$ in the p-$Bi_{0.5}Sb_{1.5}Te_3$ films formed at various process variables, and $S(T)$ and $\sigma(T)$ in the bulk sample (Figure 2, curves *5, 10*) with the same composition made by the vertical zone leveling method.

Compared with the bulk sample, dependences $S(T)$ in films become weaker, in particular, at temperatures below $T_D$, and the values of $S$ grow (Figure 2). The highest Seebeck coefficient $S$ is observed in an unannealed

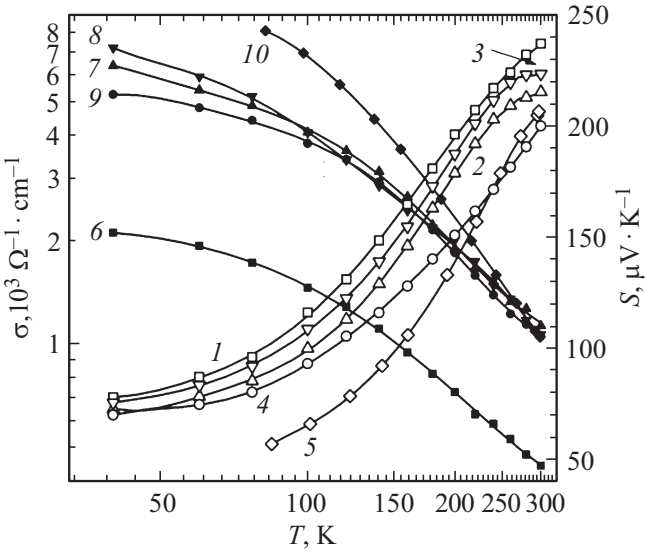


**Figure 2.** Temperature dependences of the Seebeck coefficient $S$ (curves *1–4*) and electric conductivity $\sigma$ (*6–9*) in the p-$Bi_{0.5}Sb_{1.5}Te_3$ solid solution films and bulk sample with the same composition $S$ (*5*) and $\sigma$ (*10*). *1, 6* — discrete evaporation, substrate — unannealed polyimide; *2, 7* — discrete evaporation, annealed polyimide; *3, 8* — discrete evaporation, substrate — annealed mica; *4, 9* — thermal evaporation, unannealed polyimide; *5, 10* — bulk sample made by the vertical zone leveling method.

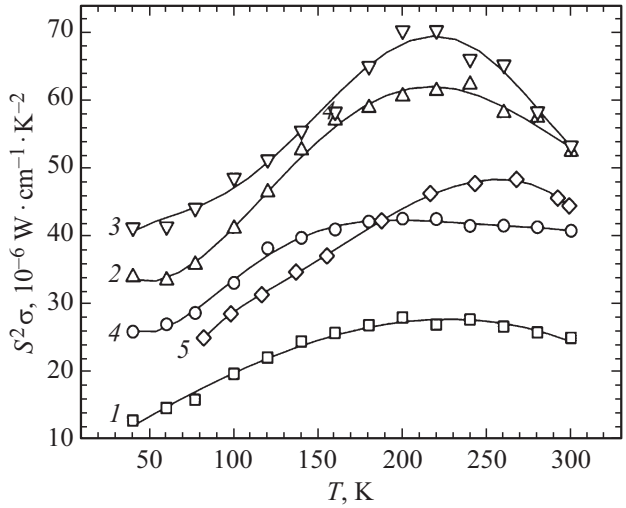


**Figure 3.** temperature dependence of $S^2\sigma$ in the p-$Bi_{0.5}Sb_{1.5}Te_3$ films. Curve *1* — discrete evaporation, unannealed polyimide substrate; *2* — discrete evaporation, annealed polyimide; *3* — discrete evaporation, annealed mica substrate; *4* — thermal evaporation, unannealed polyimide; *5* — bulk sample made by the vertical zone leveling method.

laminated film during the discrete evaporation on the polyimide substrate (Figure 2, curve *1*). In the annealed film deposited in the same conditions (Figure 2, curve *2*), the Seebeck coefficient decreases throughout the measured temperature range. Employment of the mica substrate for the discrete evaporation in the annealed film leads to a slight reduction of $S$ (Figure 2, curve *3*). Considerable reduction of the Seebeck coefficient was achieved in the unannealed film deposited by thermal evaporation onto the polyimide substrate (Figure 2, curve *4*).

When other technique is used, the temperature dependences $S(T)$ (Figure 2) in the TI films are defined by the energy [4,5,9] during carrier scattering at grain interfaces in the laminated p-$Bi_{0.5}Sb_{1.5}Te_3$ polycrystalline films. $|r_{\text{eff}}|$ in $\tau(E) \propto E^{r\text{eff}}$ grows, which corresponds to the increase in the Seebeck coefficient $S$ (Figures 1 and 2).

The highest electric conductivity in a film was observed during the discrete deposition onto mice followed by annealing (Figure 2, curve *8*). The Seebeck coefficient in this film decreased insignificantly (Figure 2, curve *3*) compared with the unannealed film on the polyimide substrate (Figure 2, curve *1*). In the p-$Bi_{0.5}Sb_{1.5}Te_3$ bulk solid solution, the electric conductivity was higher and $\sigma(T)$ was sharper throughout the temperature range than in films (Figure 2, curves *6–10*).

High electric conductivity $\sigma(T)$ (Figure 2, curve *8*) provides increase in the power factor (Figure 3, curve *3*) in the annealed film on mica, while the power factor in the unannealed film on polyimide with low electric conductivity decreases sharply (Figure 3, curve *1*). Varying of the film deposition variables leads to optimization of scattering processes affecting the dependence of $\sigma$ on $r_{\text{eff}}$ (Figure 4).

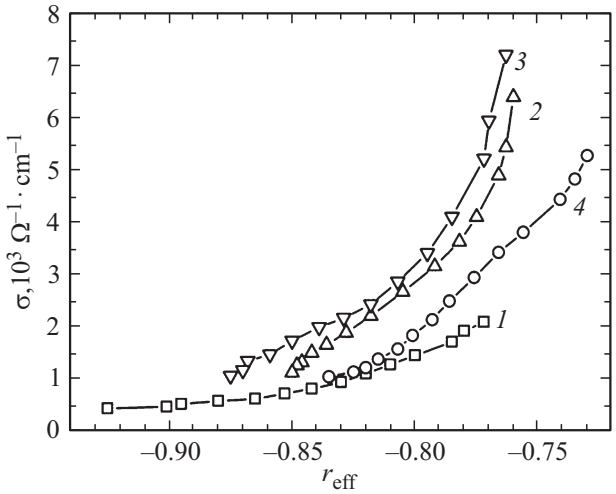


**Figure 4.** Dependences of $\sigma$ on $r_{\text{eff}}$ in the p-$Bi_{0.5}Sb_{1.5}Te_3$ films. Samples are denoted as in Figure 1.

High electric conductivity and power factor in the annealed film on mica (Figure 2, curve *8*; Figure 3, curve *3*) at $r_{\text{eff}}$ from $-0.763$ to $-0.875$ that are the best values (Figure 4, curve *3*) may be explained by the increase in the contribution of surface electric conductivity in accordance with [5,26]. The largest increase of $r_{\text{eff}}$ in absolute value from $-0.772$ to $-0.925$ (Figure. 4, curve *1*) was achieved in the unannealed film on polyimide with low values of $\sigma$ and power factor (Figure 2, curve *6*; Figure 3, curve *1*), which is explained by reduction of the surface electric conductivity [5,26]. In the p-$Bi_{0.5}Sb_{1.5}Te_3$ bulk sample, $r_{\text{eff}}$ was lower in absolute value that in film and equal to $-0.75$ and $-0.78$ at 77 and 300 K [27].

## 5. Thermal conductivity

Total thermal conductivity $\kappa$ of the p-$Bi_{0.5}Sb_{1.5}Te_3$ films may be written as $\kappa = \kappa_L + \kappa_e$, where $\kappa_L$ and $\kappa_e$ are thermal conductivity of the lattice and electronic thermal conductivity, respectively. In accordance with the Wiedemann-Franz law, electronic thermal conductivity $\kappa_e$ and electric conductivity $\sigma$ are interconnected as $\kappa_e = L(r, \eta) \cdot \sigma T$, where $L(r, \eta)$ is the Lorentz number. Calculations of $L(r, \eta)$ included $r_{\text{eff}}(\eta)$ (Figure 5).

Significant reduction of $\kappa$ and $\kappa_L$ in films accompanied with weakening of temperature dependences $\kappa(T)$ and $\kappa_L(T)$ was observed during the discrete deposition of the p-$Bi_{0.5}Sb_{1.5}Te_3$ films (Figures 5 and 6, curves *1, 2*) on the polyimide substrate. The largest reduction of $\kappa$ and $\kappa_L$ throughout the studied temperature range was achieved in the unannealed film (Figures 5 and 6, curve *1*).

$\kappa$ and $\kappa_L$ grow and the slopes of $\kappa(T)$ and $\kappa_L(T)$ become sharper in the low temperature area in the annealed p-$Bi_{0.5}Sb_{1.5}Te_3$ films deposited by the discrete evaporation on mica substrates (Figures 5 and 6, curve *3*). High values of $\kappa$ and $\kappa_L$ were also observed in the unannealed p-$Bi_{0.5}Sb_{1.5}Te_3$ films formed by the thermal evaporation on the polyimide substrate (Figures 5 and 6, curve *4*). Values of the total thermal conductivity $\kappa$ and lattice thermal conductivity $\kappa_L$ (Figures 5 and 6) agree well with the data for films deposited onto the polyimide substrates by the thermal evaporation method [28], and for the composite p-$Bi_{0.52}Sb_{1.48}Te_3$ solid solutions [5].

Temperature dependences of $\kappa_e$ (Figure 6, inset) are defined by $\sigma(T)$ (Figure 2) that consists of the surface metallic and bulk electric conductivities and also depends on $L(r_{\text{eff}}, \eta)$ (Figure 5, inset). At low temperatures, increase in $\kappa_e$ in the range from 40 to 80 K (Figure 6, inset, curves 2–4) comes with significant reduction of slopes of $\sigma(T)$ compared with 100–300 K

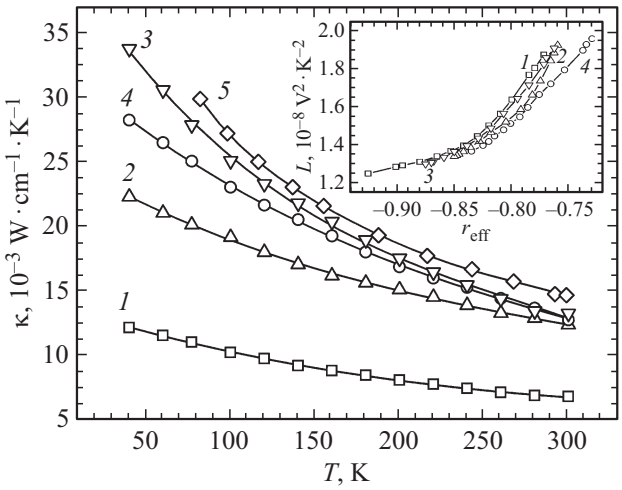


**Figure 5.** temperature dependences of the $\kappa$ films (curves *1–4*) and (*5*) the p-$Bi_{0.5}Sb_{1.5}Te_3$ bulk sample. Inset — dependences of the Lorentz number $L$ on $r_{\text{eff}}$ in the p-$Bi_{0.5}Sb_{1.5}Te_3$ films. Samples are denoted as in Figure 4.

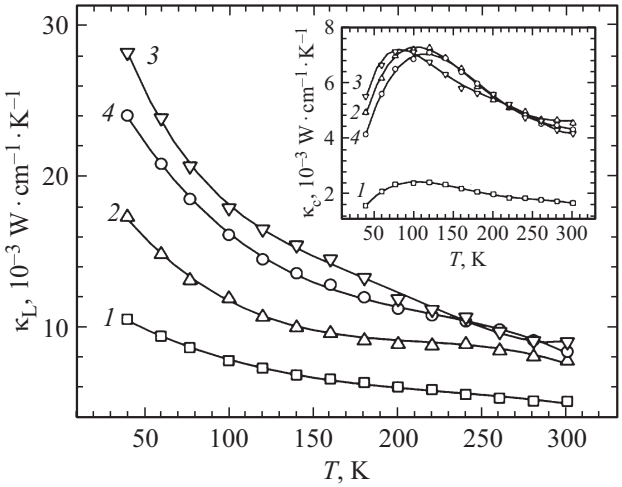


**Figure 6.** temperature dependences of the thermal conductivity $\kappa_L$ (curves *1–4*) and electronic thermal conductivity $\kappa_e$ (*1–4* in the inset) of the p-$Bi_{0.5}Sb_{1.5}Te_3$ films. Samples are denoted as in Figure 1.

(Figure 2), while $d\ln\sigma/d\ln T = 0.1$ in the temperature range of $T = (40-80)$ K and $d\ln\sigma/d\ln T = (1-1.2)$ at $T = (100-300)$ K.

Behavior of $\sigma(T)$ is explained by the increase in the contribution of the surface metallic electric conductivity as a result of the optimization of electron scattering on the intrinsic antisite defects $Bi_{Te}$ and impurity defects of substitution $Sb \to Bi$ in the p-$Bi_{0.5}Sb_{1.5}Te_3$ solid solution when the film deposition technique is changed. In addition, singularity on $\kappa_e(T)$ at low temperatures in the p-$Bi_{0.5}Sb_{1.5}Te_3$ films is explained by the strengthening of the energy dependence of relaxation time $\tau$ due to the growth of $|r_{\text{eff}}|$ that was used during calculation of the Lorentz number (Figures 3 and 5, insets).

## 6. Thermoelectric figure of merit

The highest thermoelectric figure of merit $Z$ is observed in the p-$Bi_{0.5}Sb_{1.5}Te_3$ films formed by the discrete evaporation on the polyimide substrate (Figure 7, curve *2*) and mica substrate (Figure 7, curve *3*) exposed to heat treatment.

Within 200−300 K, values of $Z$ in these films are close to (Figure 7, curves *2, 3*), the maximum figure of merit is $Z_{\max} = 4.5 \cdot 10^{-3}\,\text{K}^{-1}$ at $T = 240$ K, and the mean values is equal to $\langle Z\rangle = 4.35 \cdot 10^{-3}\,\text{K}^{-1}$. Increase in $Z$ in the range of $T = (200-300)$ K in the film on polyimide is defined by low total thermal conductivity $\kappa$ and lattice thermal conductivity $\kappa_L$, (Figure 5−7, curves *2*), and in the film on mice is associated with the growth of the Seebeck coefficient and power parameter throughout the studied temperature range (Figures 2 and 4, curves *3*). With temperature reduction at $T < 200$ K, $Z$ increases in the film on the polyimide substrate due to the growth the power factor and considerable reduction of $\kappa$ and $\kappa_L$ (Figures 4−7, curves *2*). Mean values of $\langle Z\rangle$ in the temperature range 100−200 K in the films are equal to $(3.2\cdot$ and $2.8)\cdot 10^{-3}\,\text{K}^{-1}$, respectively (Figure 7, curves *2, 3*). At low temperatures $T < 160$ K, close values of $Z$ were obtained during the discrete deposition of the unannealed films on polyimide and annealed films on mica (Figure 7, curves *1, 3*). However, as the temperature in the unannealed films on polyimide grows, $Z$ decreases to $Z_{\max} = 3.75 \cdot 10^{-3}\,\text{K}^{-1}$ at $T = 260$ K due to the electric conductivity reduction, despite the low thermal conductivity (Figures 2 and 5−7, curves *1*).

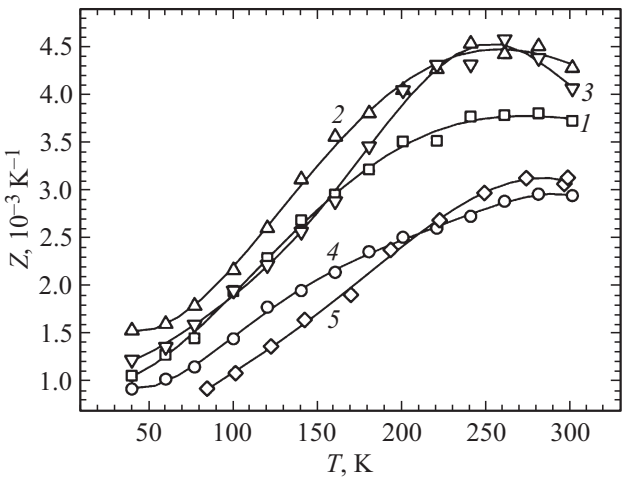


**Figure 7.** Temperature dependence of $Z$ in the p-$Bi_{0.5}Sb_{1.5}Te_3$ films. Samples are denoted as in Figure 4.

In the unannealed film on polyimide deposited by thermal evaporation, the figure of merit decreases to $Z_{\max} = 3.25 \cdot 10^{-3}\,\text{K}^{-1}$ at $T = 300$ K (Figure 7, curve *4*) due to the growth of $\kappa$ and $\kappa_L$, reduction of the Seebeck coefficient and power factor (Figures 2, 3, 5 and 6, curves *4*).

Analysis of the temperature dependences of the thermoelectric figure of merit shows that the values of $Z$ increase in the p-$Bi_{0.5}Sb_{1.5}Te_3$ films at the optimum values of $r_{\text{eff}}$ (Figures 1 and 4) to which the optimum dependence $\tau(E) \propto E^{r\text{eff}}$ corresponds. In the temperature range of 200−300 K, growth of $Z$ is observed in the annealed films obtained by the discrete evaporation on the polyimide and mica substrates (Figure 7, curves *2, 3*) at the optimum values of $r_{\text{eff}} = (-0.875)-(-0.83)$. In the low temperature range of 100−200 K, reduction of $Z$ was achieved in the p-$Bi_{0.5}Sb_{1.5}Te_3$ film during the discrete deposition onto polyimide (Figure 7, curve *2*) at $r_{\text{eff}} = (-0.84)-(-0.785)$.

## 7. Conclusion

Thermoelectric properties were studied in the temperature range of 40−300 K in the p-$Bi_{0.5}Sb_{1.5}Te_3$ TI films formed on the polyimide and mica substrates by the discrete deposition and thermal evaporation methods. Measurement range of the effective scattering parameter $r_{\text{eff}}$ was determined in the energy dependence of the relaxation time $\tau(E) \propto E^{r\text{eff}}$, in which the increase in the thermoelectric figure of merit $Z$ was achieved. The optimum values of $r_{\text{eff}} = (-0.875)-(-0.83)$ for the temperature range $(200-300)$ K; in the low temperature range of 100−200 K - $r_{\text{eff}} = (-0.84)-(-0.785)$.

It is shown that at the optimum values of $r_{\text{eff}}$, the highest $Z_{\max} = 4.5 \cdot 10^{-3}\,\text{K}^{-1}$ at $T = 240$ K is observed in the annealed films formed by the discrete deposition onto the polyimide and mica substrates. Growth of $Z$ at the optimum values of $r_{\text{eff}}$ is defined by low thermal conductivity in the film on polyimide, and by the increase in the Seebeck coefficient and power factor in the film on mica. Growth of the Seebeck coefficient associated with the energy filtration effect of carriers is accompanied by the increase in $|r_{\text{eff}}|$ that is affected by both bulk and surface carriers.

Increase in $r_{\text{eff}}$ compared with the optimum values is accompanied by the reduction of the figure of merit to $Z_{\max} = 3.75 \cdot 10^{-3}\,\text{K}^{-1}$ at $T = 260$ K due to the electric conductivity reduction in the unannealed film during the discrete deposition onto the polyimide substrate. When the values of $r_{\text{eff}}$ are lower than the optimum values

in the unannealed film on polyimide deposited by the thermal evaporation, the figure of merit decreases to $Z_{max} = 3.25 \cdot 10^{-3}\,K^{-1}$ at $T = 300\,K$ due to the growth of thermal conductivity.

### Conflict of interest

The authors declare no conflicts of interest.

## References


[1] M.Z. Hasan, C.L. Kane. Rev. Mod. Phys. **82**, *4*, 3045 (2010).
[2] Y.L. Chen, J.G. Analytis, J.-H. Chu, Z.K. Liu, S.-K. Mo, X.L. Qi, H.J. Zhang, H. Lu, X. Dai, Z. Fang, S.C. Zhang, I.R. Fisher, Z. Hussain, Z.-X. Shen. Sci. **325**, *5937*, 178 (2009).
[3] M.J. Gilbert. Commun. Phys. **4**, *1*, 70 (2021).
[4] J.P. Heremans, R.J. Cava, N. Samarth. Nature Rev. Mater. **2**, *10*, 17049 (2017).
[5] S.Y. Matsushita, K. Ichimura, K.K. Huynh, K. Tanigaki. Phys. Rev. Mater. **5**, *1*, 014205 (2021).
[6] K. Nomura, A.H. MacDonald. Phys. Rev. Lett. **98**, *7*, 076602 (2007).
[7] K. Nomura, M. Koshino, S. Ryu. Phys. Rev. Lett. **99**, *14*, 146806 (2007).
[8] T.-H. Liu, J. Zhou, M. Li, Z. Ding, Q. Song, B. Liao, L. Fu, G. Chen. Proc. Natl. Acad. Sci. **115**, *5*, 879 (2018).
[9] J. Zhou, X. Li, G. Ghen, R. Yang. Phys. Rev. B **82**, *11*, 115308 (2010).
[10] N. Xu, Y. Xu, J. Zhu. npj Quantum Mater. **2**, *1*, 51 (2017).
[11] J. Zhang, C.-Z. Chang, Z. Zhang, J. Wen, X. Feng, K. Li, M. Liu, K. He, L. Wang, X. Chen, Q.-K. Xue, X. Ma, Y. Wang. Nature Commun. **2**, *1*, 574 (2011).
[12] T. Knispel, W. Jolie, N. Borgwardt, J. Lux, Z. Wang, Y. Ando, A. Rosch, T. Michely, M. Grüninger. Phys. Rev. B **96**, *19*, 195135 (2017).
[13] H. Nam, Y. Xu, I. Miotkowski, J.F. Tian, Y.P. Chen, C. Liu, M.Z. Hasan, W.G. Zhu, G.A. Fiete, C.-K. Shih. J. Phys. Chem. Solids **128**, 251 (2019).
[14] J. Zheng, Y. Kodera, X. Xu, S. Shin, K.M. Chung, T. Imai, R.V. Ihnfeldt, J.E. Garay, R. Chen. J. Appl. Phys. **130**, *23*, 235106 (2021).
[15] P. Puneet, R. Podila, M. Karakaya, S. Zhu, J. He, T.M. Tritt, M.S. Dresselhaus, A.M. Rao. Sci. Rep. **3**, *1*, 3212 (2013).
[16] B. Poudel, Q. Hao, Y. Ma, Y. Lan, A. Minnich, B. Yu, X. Yan, D. Wang, A. Muto, D. Vashaee, X. Chen, J. Liu, M.S. Dresselhaus, G. Chen, Z. Ren. Sci. **320**, *5876*, 634 (2008).
[17] K.H. Park, M. Mohamed, Z. Aksamija, U. Ravaioli. J. Appl. Phys. **117**, *1*, 015103 (2015).
[18] M.H. Francombe. Brit. J. Appl. Phys. **9**, *10*, 415 (1958).
[19] D.L. Medlin, Q.M. Ramasse, C.D. Spataru, N.Y.C. Yang. J. Appl. Phys. **108**, *4*, 043517 (2010).
[20] N. Virk, O.V. Yazyev. Sci. Rep. **6**, *1*, 20220 (2016).
[21] Yu.A. Boikov, B.M. Goltsman, S.F. Sinenko. PTE *2*, 230 (1975).
[22] L.N. Lukyanova, Y.A. Boikov, V.A. Danilov, O.A. Usov, M.P. Volkov, V.A. Kutasov. Semicond. Sci. Technol. **30**, *1*, 015011 (2015).
[23] L.N. Lukyanova, I.V. Makarenko, O.A. Usov, P.A. Dementev. Semicond. Sci. Technol. **33**, *5*, 055001 (2018).
[24] T. Chiba, S. Takahashi. J. Appl. Phys. **126**, *24*, 245704 (2019).
[25] Y.L. Chen, J.-H. Chu, J.G. Analytis, Z.K. Liu, K. Igarashi, H.-H. Kuo, X.L. Qi, S.K. Mo, R.G. Moore, D.H. Lu, M. Hashimoto, T. Sasagawa, S.C. Zhang, I.R. Fisher, Z. Hussain, Z.X. Shen. Sci. **329**, *5992*, 659 (2010).
[26] Y. Xu, I. Miotkowski, C. Liu, J. Tian, H. Nam, N. Alidoust, J. Hu, C.-K. Shih, M.Z. Hasan, Y.P. Chen. Nature Phys. **10**, *12*, 956 (2014).
[27] L.N. Lukyanova, V.A. Kutasov, V.V. Popov, P.P. Konstantinov. Phys. Solid State **46**, *8*, 1404 (2004).
[28] L.M. Goncalves, C. Couto, P. Alpuim, A.G. Rolo, F. Völklein, J.H. Correia. Thin Solid Films **518**, *10*, 2816 (2010).


*Translated by E.Ilinskaya*